Comparative Study on Finite Element Analysis & System Model Extraction for Non-Resonant 3-DoF Microgyroscope

Rana I. Shakoor
Pakistan Institute of Engineering & Applied Sciences, Islamabad
Pakistan
iqtidar@pieas.edu.pk
Tele: +9251 2207381
Fax: +92 51 2208070

Shafaat A. Bazaz
GIK Institute of Engineering Sciences & Technology, Topi,
Pakistan
bazaz@giki.edu.pk

Y. Lai
Queens University,
Kingston, ON, Canada,
K7L3N6
lai@me.queensu.ca

M. M. Hasan
Pakistan Institute of Engineering & Applied Sciences, Islamabad
Pakistan
masoodh@pieas.edu.pk

***Abstract*— This paper reports a comparative study of full transient start up analysis of a Non-Resonant Micromachined Gyroscope using Finite Element Analysis (FEA) and System Model Extraction (SME) techniques. FEA is a popular numerical technique based on Finite Element Method (FEM) for carrying out different engineering analyses. But one of the major disadvantages of this FEA is its computational time. While running multiple optimization analyses with a FE Solver, it may take days, weeks and possibly months depending on extent of optimization. In this study we initially analyzed the MEMS based microgyro on a device level using FEM. We determined the natural frequencies of the gyro along with the both static and dynamic responses of the gyro. After these device level simulations in FEA we switched to the system level simulation. Using SME we generated system model of the gyro with system level components and run a full transient startup response analysis of the device by incorporating that extracted model in INTELLISUITE circuit simulator SYNPLE. When we compared the computational time required by both techniques, we found that SME with SYNPLE is orders of magnitude faster than FEA.**

***Index Terms*— Finite element method, Micromachined Gyroscope, MEMS, Reduce Order Macromodel.**

I. Introduction

MICROMACHINED inertial sensors are a very versatile group of sensors with applications in many areas. They measure either linear acceleration (along one or several axes) or angular motion about one or several axes. The former is usually referred to as an accelerometer, the latter as a gyroscope. Until recently, medium to high performance inertial sensors were restricted to applications in which the cost of these sensors was not of crucial concern, such as military and aerospace systems. But the advancements in the micromachining technology has generated the possibility of producing precision inertial sensors at a price that allows their usage in cost-sensitive consumer applications. Conventional rotating wheel as well as precision fiber-optic and ring laser gyroscopes are all too expensive and too large for use in most emerging applications. Micromachining can shrink the sensor size by orders of magnitude reducing their fabrication cost significantly and allowing the electronics to be integrated on the same silicon chip [1].

A variety of such applications already exists, mainly in the automotive industry for safety systems such as airbag release, seat belt control, active suspension, and traction control. In military application these inertial sensors are being used as inertial guidance and smart ammunition. Medical applications include patient monitoring, for example, for Parkinson's disease. Many products, however, are currently in their early design and commercialization stage, and only one's imagination limits the range of applications.

In section II, operating principle of microgyroscope along with the conventional resonant design approach has been presented. Same section II comprehends some issues with conventional resonant gyroscopes including Quadrature error and anisoelasticity to justify our 3-DOF Non-resonant approach. Section III covers the background theory of Non-resonant approach and proposed microgyroscope design with 2-DoF drive mode and 1-DoF sense mode oscillators along with its lumped model and resultant equation of motions. Section IV covers some basics of System Model Extraction technique and its methodology. Prototype modeling and comparison of simulation results achieved by FEM and SME techniques are presented in section V and VI respectively.

Manuscript received June 21, 2008. This work was supported in part by the Higher Education Commission of Pakistan through Indigenous 5000 Scholarship and IRSIP.

Rana I. Shakoor is pursuing his PhD studies at Department of Chemical and Materials Engineering, Pakistan Institute of Engineering and Applied Sciences, (PIEAS) Islamabad, Pakistan. Telephone: +92 51 2207381, fax: +92 51 2208070 iqtidar@ pieas.edu.pk.

Shafaar A. Bazaz is with GIK Institute of Engineering Sciences & Technology, Topi, Pakistan bazaz@giki.edu.pk

Y. Lai is with Queens University, Kingston, ON, Canada, K7L3N6 lai@me.queensu.ca

M. M. Hasan is with Pakistan institute of Engineering & Applied Sciences, Islamabad Pakistan masoodh@pieas.edu.pk

II. CONVENTIONAL MICROMACHINED GYROSCOPE

A. Operating Principle

Almost in all reported micromachined gyroscopes, the sensitive element can be represented as an inertia element and elastic suspension with two prevalent degrees of freedom as shown in Fig.1. All vibratory gyroscopes are based on the principle that the Coriolis forces produced by the rotation of the gyro cause a transfer of energy between two vibration modes of the gyro structure. The massive inertia element, Proof Mass, is driven into one of its modes with prescribed amplitude which is called Primary Mode. When this proof mass rotates about a particular fixed axis, sensitive axis, the resultant Coriolis force causes the proof mass to move in different mode, secondary mode, orthogonal to both sensitive axis and drive axis.

Coriolis force is a fictitious force exerted on a body when it moves in a rotating reference frame. It is called a fictitious force because it does not appear when the motion is observed in Inertial Frame of Reference. General expression for Coriolis acceleration is

$$\vec{a}_c = -2\vec{\Omega}\times\vec{\upsilon} \qquad (1)$$

where $\vec{\upsilon}$, is the translational velocity of the particle in the

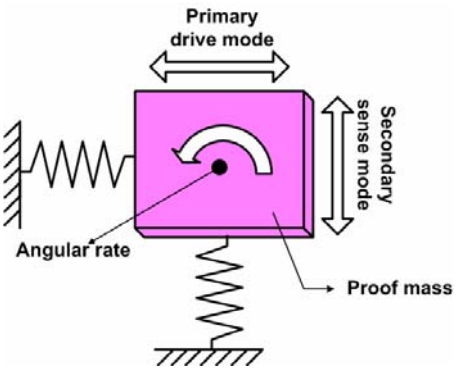

Fig. 1. Operating principle of resonant micromachined vibratory gyroscope [7].

rotating system, and $\vec{\Omega}$ is the angular velocity vector. The minus sign arises from the traditional definition of the cross product (right hand rule), and from the sign convention for angular velocity vectors. The equation may be multiplied by the mass of the relevant object to produce the Coriolis force

$$\vec{F}_c = -2m\vec{\Omega}\times\vec{\upsilon} \qquad (2)$$

The resulted force is directly proportional to the rate of rotation. This effect is the basic operating principle underlying all vibratory structure gyroscopes.

B. Issue in conventional micromachined gyroscopes

To achieve the maximum gain the conventional gyroscopes are operated near at or near the peak of the response curve which is achieved by mode matching. However system becomes very sensitive to variation in system parameters causing a shift in the resonant frequency. However fabrication flaws and environmental changes drastically affect the suspension stiffness. Both the geometry and the material properties of MEMS device vary due to variation in photolithography and etching processes, deposition conditions, and residual stresses. So it becomes very hard to match the suspension stiffness which finally hinders the resonance frequencies of both drive and sense modes to match. Generally post-processing techniques for example laser trimming, or sophisticated control electronics are used to tune the resonance frequencies for mode-matching.

Now consider another effect of fabrication flaw and residual stresses in MEMS gyroscopes, that is mismatch in drive and sense direction stiffness, which in turn results in minimum and maximum stiffness axes to occur in the plane of oscillation. Because of these slight asymmetries in structure due to random scatter of imperfections, these maximum and minimum axes are likely to deviate from the drive and sense drive directions. This results in misalignment of the intended and actual principle axes of oscillation, causing both anisoelasticity in the gyroscopes structure and dynamic cross-coupling between the drive and sense directions. Both of these factors play a major role in limiting the performance of the gyroscopes [2]-[4].

III. NON-RESONANT MICROMACHINED VIBRATORY GYROSCOPES (MVG)

For the last several years, research is being carried out to enhance the inherent robustness of Micromachined vibratory rate gyroscopes against the structural and environmental parameter variations. Several new classes of MEMS rate gyroscopes with increased robustness has been introduced structurally, effectively shifting the complexity from the control electronics to the structural design of gyroscopes dynamical parameters [5]. A dynamical system with a wide-bandwidth frequency response can be achieved by: Expanding the system design space by increasing the degree-of-freedom (DoF) of the drive and sense mode oscillatory system; utilizing multiple drive-mode oscillators with incrementally spaced resonant frequencies.

Wide bandwidth frequency responses in drive and sense-modes play a vital role in enhancing the robustness. So utilizing a 3DoF dynamic system as opposed to 2-DoF system conventionally used in Resonant MVG is one approach to increase the bandwidth of vibratory rate gyroscope [6]-[7]. This design approach aims to utilize resonance either in drive mode or sense mode to improve sensitivity while maintaining the robust operational characteristics. This could be achieved, for example by designing structurally decoupled 1-DoF and 2-DoF oscillator in sense and drive-modes. There will be two resonance peaks in the frequency response of 2-DoF drive-mode oscillator with a flat region between both peaks which defines the operational frequency region. Resonance frequency of 1-DoF sense mode oscillator is designed in way to overlap the flat frequency region of drive-mode. Thus the device is operated at the resonance frequency of 1-DoF oscillator, while 2-DoF oscillator amplitude is inherently

constant with in the same frequency band.

The overall 3-DoF micromachined vibratory gyroscopes consist of two interconnected proof masses m_1 and m_2 as shown in Fig. 2. Mass m_1 is excited in the drive direction (X-Axis) whereas it is constrained to oscillate in sense direction. For the driving purpose of the gyroscope, a very famous comb drive actuation mechanism is being used. This is very well proven mechanism to obtain large linear displacements. However large drive voltages are required and the resultant force of comb drive is low. Mass m_2 can oscillate both in drive and sense direction (Y-Axis). In this way the gyroscope dynamical system consists of a 2-DoF drive mode oscillator

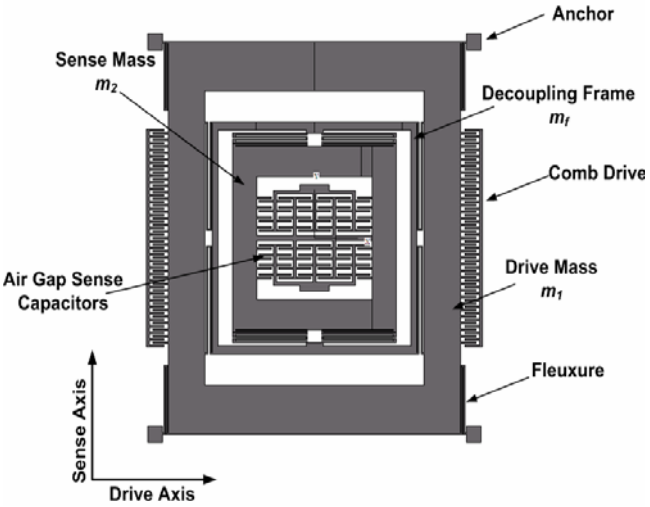

Fig. 2. 3-DoF Non-Resonant Micromachined Vibratory Gyro with 2-DoF Drive mode and 1-DoF sense mode oscillator.

along with 1-DoF Sense-mode oscillator. Mass m_2 thus forms the passive mass of the 2-DoF Drive mode oscillator and act as the vibration absorber of mass m_1.

Thus the equation of motion of m_1 and m_2 when subjected to an angular rate of Ω_z about the z-Axis become:

$$\left.\begin{aligned} m_1\ddot{x}_1 + c_{1x}\dot{x}_1 + k_{1x}x_1 &= k_{2x}(x_2 - x_1) + m_1{\Omega_z}^2 x_1 + F_d(t) \\ (m_2 + m_f)\ddot{x}_2 + c_{2x}\dot{x}_2 + k_{2x}(x_2 - x_1) &= (m_2 + m_f){\Omega_z}^2 x_2 \\ m_2\ddot{y}_2 + c_{2y}\dot{y}_2 + k_{2y}y_2 &= m_2{\Omega_z}^2 y_2 - 2m_2\Omega_z\dot{x}_2 - m_2\dot{\Omega}_z x_2 \end{aligned}\right\} \quad (3)$$

Where m_f is the mass of decoupling frame, F_d is the driving electrostatic force applied to the active mass at the driving frequency.

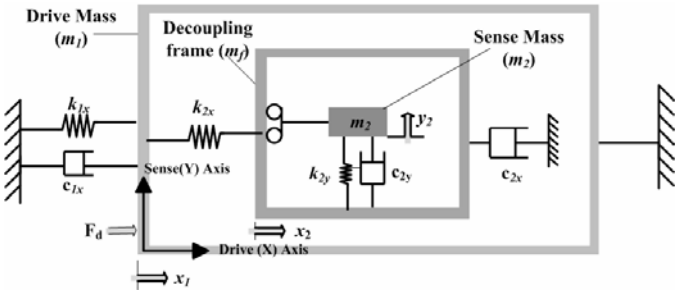

Fig. 3. Lumped mass-spring model of the 3-DoF

The Coriolis force that excites the mass m_2 in the sense direction is $2m_2\Omega_z\dot{x}_2$ and the Coriolis response of m_2 in the sense direction (y) is detected for angular rate measurement.

IV. System Model Extraction (SME)

SME is a technique by which a full three dimensional meshed numerical model of a multi-conductor electromechanical device without the dissipation can be converted into reduce order analytical macromodel. This can then be inserted as a black-box element into a mixed signal circuit simulator. This process is based upon energy method approach in which analytical models for each of the energy domain of the system is constructed and all forces as the gradients of the energy are determined [9].

A. SME Methodology

Our first task is to reduce the degree of freedom of the system. We constrain the motion of the system to a linear superposition of selected set of deformation shape. This set will act as our basis set of motion. Next we must construct analytical macromodels of each of the energy domains of the system. In the case of capacitive electromechanical systems, these consist of electrostatic, electrostatic, and kinetic energy domain. These macromodels will be analytical functions of the generalized coordinates. We can then use lagrangian mechanics to construct the equation of motion for the system in terms of its generalized coordinates. Finally we can translate these equations of motions into an analog hardware description language, thereby constructing a black-box model of the electromechanical system that can be inserted in to an analog circuit simulator [9]. Fig. 4 shows a systematic methodology to create a macromodel.

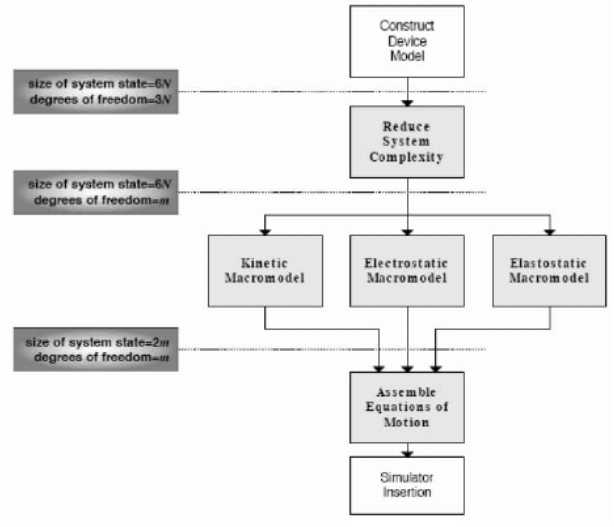

Fig. 4. Creation of Macromodel [9].

V. Prototype Modeling

A prototype 3-DoF gyroscope was designed for

experimental demonstration of the design concept with the following dynamical system parameters. The proof mass values are $m_1 = 3.86\times10^{-7}$ kg and $m_2 = 1.346\times10^{-7}$ kg and the decoupling frame mass is $m_f = 4.8\times10^{-8}$ kg. The spring constants for folded flexure are $k_{1x} = 65.10$ N/m, $k_{2x} = 12.32$ N/m and $k_{2y} = 14.45$ N/m calculated by finite element method (FEM) using Thermoelectromechanical (TEM) Analysis module of MEMS Design software IntelliSuite. These spring constants can be approximated analytically by the formulae explained in the mechanical design implementation of suspension design. For example for $k_{1x} = 65.10$ N/m, we can approximate this stiffness by putting the relevant values in

$$k_1x = \frac{4}{2}\left(\frac{1}{2}\frac{3EI}{\frac{L_{1x}^3}{2}}\right) = \frac{2Etw^3}{L_{1x}^3} \qquad (4)$$

Where $t = 20\mu m$ is the beam thickness, $w = 8\mu m$ is the beam width and $L_{1x} = 410\mu m$ is the length of beam whereas Young's Modulus $E = 214GPa$ was assumed for the Ni as our structural layer is of Ni in the process of MetalMUMPs, we used for the prototype fabrication. The calculated $k_{1x} = 63.59$ N/m is in good agreement with $k_{1x} = 65.10$ N/m calculated by IntelliSuite. Simulation results can be further refined to reduce this error by mesh refining but this exponentially increases the computational time. So an optimized mesh size gives FEA results which are accurate enough achieved through a reasonable computational time.

Thus for drive mode Oscillator, the active and passive proof mass values become $m_{1x} = 3.86\times10^{-7}$ kg and $m_{2x} = (m_2 + m_f) = 1.826\times10^{-7}$ kg. In the drive mode, the resonant frequencies of the isolated active and passive mass-spring systems are $\Omega_{1x} = \sqrt{k_{1x}/m_{1x}} = 2.068kHz$ and $\Omega_{2x} = \sqrt{k_{2x}/(m_2 + m_f)} = 1.308kHz$, respectively and resulting frequency ratio will be $\lambda_x = \Omega_{2x}/\Omega_{1x} = 0.632$ and a mass ratio of $\mu_x = (m_2 + m_f)/m_1 = 0.47$. With these parameters the location of the two expected resonance peaks in the drive mode frequency response were calculated as $\Omega_{x\text{-}n_1} = 1.16kHz$ and $\Omega_{x\text{-}n_2} = 2.34kHz$ based on the relation [10]

$$\left.\begin{aligned}\Omega_{x\text{-}n_1} &= \sqrt{1/2(1+\mu_x+1/\lambda_x^2 - \sqrt{(1+\mu_x+1/\lambda_x^2)^2 - 4/\lambda_x^2})}\,\Omega_{2x}\\ \Omega_{x\text{-}n_2} &= \sqrt{1/2(1+\mu_x+1/\lambda_x^2 + \sqrt{(1+\mu_x+1/\lambda_x^2)^2 - 4/\lambda_x^2})}\,\Omega_{2x}\end{aligned}\right\} \qquad (5)$$

VI. Simulation Results

A. FEM Results

In the drive mode frequency response, a flat region of 1.14 kHz is observed. Fig. 5 shows two resonance peaks in the drive mode frequency response which were observed at 1.18 KHz and 2.33 KHz found to be in good agreement with the theoretically estimated values of 1.16 KHZ and 2.34 KHz. When sense mode frequency response is investigated, the sense mode resonance frequency is found 1.65 kHz which is located inside the drive mode flat region, defining the operation frequency.

Fig. 6 shows 1-DoF Sense mode frequency response. After successful completion of this part of Natural frequency verifications we carried out static as well as dynamic-transient analysis for a time period of 0.001second for 6 cycles with 30 fixed time increments using IntelliSuite Thermoelectromechanical (TEM) Module.

FEA results for the applied bias voltage of 50V are shown in Fig 7. Normalized amplitude gained by both masses in drive direction is 0.0444 µm. When 50Vac at operational frequency with a rotation rate of 10 rad/sec is applied along with the bias voltage, maximum displacement achieved by the sensing mass in drive direction became 0.36 µm. This Dynamic-Transient simulation took abou et complete.

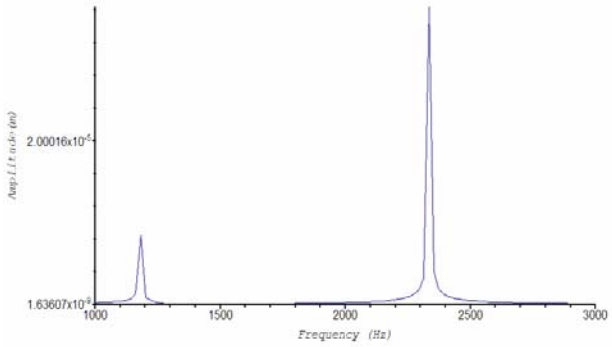

Fig. 5. 2-DoF Drive mode response showing two resonant frequencies located at 1.18KHz and 2.33KHz.

B. SME Results

Complete schematic of SYNPLE model for our 3-DoF Non-resonant MVG is shown in Fig 9 which includes drive combs, sensing gap capacitors along with the Coriolis force feed back loop. Extracted Mechanical Macromodel is linked with 5-node SYNPLE MEMS Macromodel element. Proof masses of gyroscope are driven by two electrostatic comb drives so two electrostatic comb drive elements are attached with this Macromodel to generate a driving force based on electrostatic comb drive parameters that are given to these

elements. To simulate the Coriolis effect in the gyro design, we applied a Coriolis force feedback to the representative node in sense (y) direction. The schematic of mechanical Macromodel with Coriolis force feedback is shown in Fig.8.

Rotation induced Coriolis force displaces proof mass m_2 in sense (y) direction that will be sensed by two electrostatic gap capacitors. That's why two electrostatic gap elements, top and bottom are incorporated in the SYNPLE model. This element takes the displacements in x-y plane as input variable.

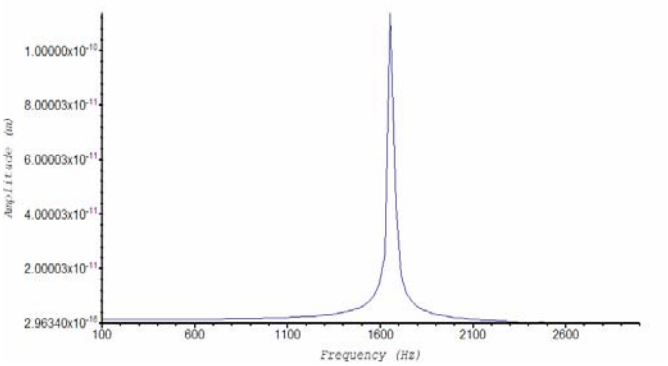

Fig. 6. 1-DoF sense mode oscillator response showing resonant peak at located at 1.65KHz

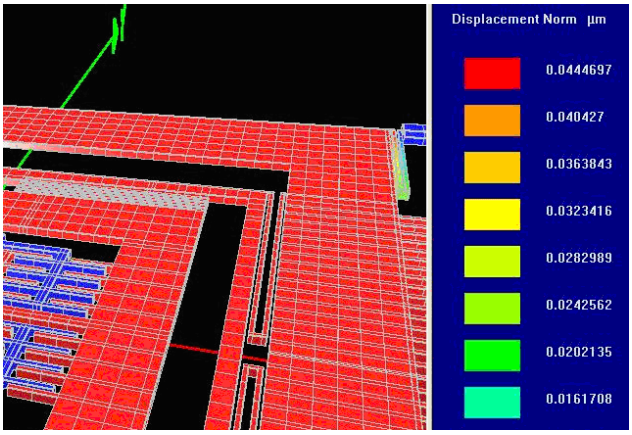

Fig. 7. FEM based Normalized 2DoF Drive direction displacements.

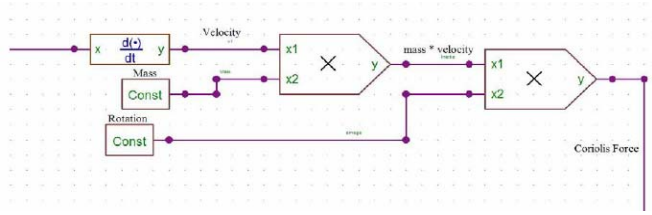

Fig. 8. Coriolis force feedback loop

.

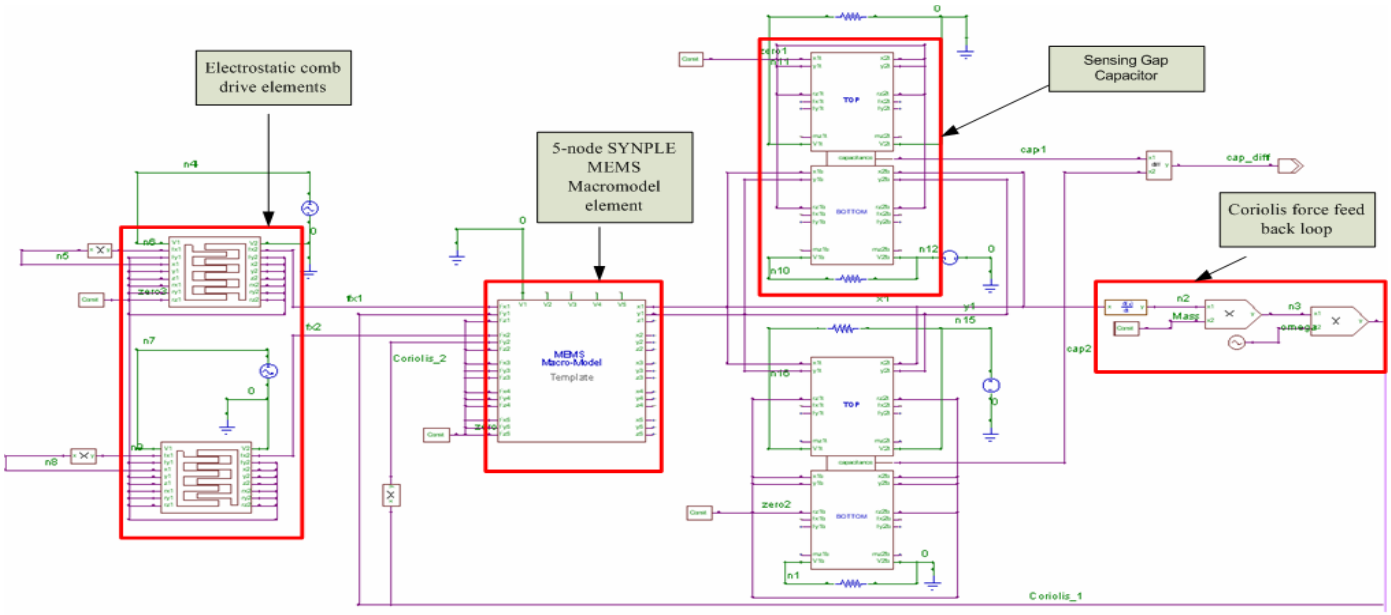

Fig. 9 Full Schematic of SYNPLE model for a 3-DoF non-resonant Micromachined Vibratory Gyro

Fig 10 shows the drive direction amplitude against the bias voltage of 50V in SYNPLE. The amplitude achieved by the mass in drive direction is .0442 µm which is in very good agreement with the FEA results .0444 µm.

Using this SYNPLE model we carried out number of dynamic-transient analysis to analyze the device behavior. The total time, taken by this SME technique while carrying out all these analyses, was two to three hours. Fig 11 and Fig.12 show the drive and sense direction Transient responses of device drawn by SYNPLE whereas Fig. 13 shows the respective differential capacitance response.

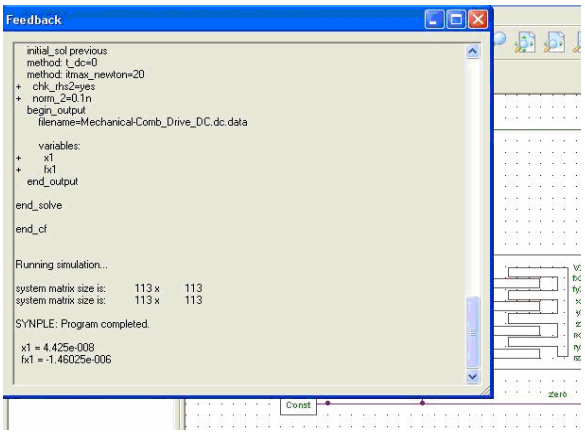

Fig. 10. SYNPLE Response against Bias voltage response.

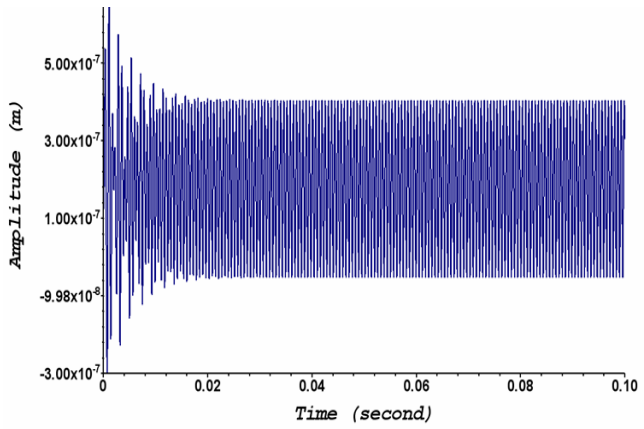

Fig. 11. SME Transient Results- Response of Drive Direction

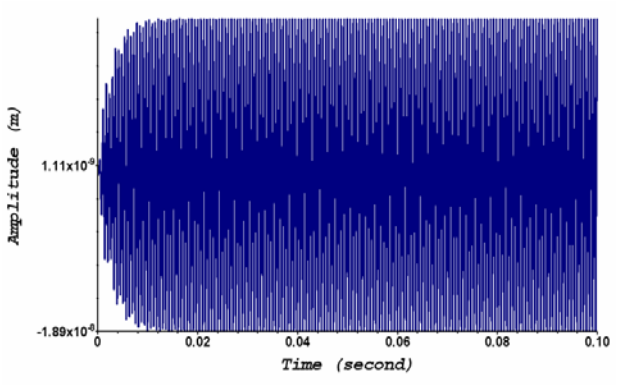

Fig. 12. SME Transient Results- Response of Sense Direction

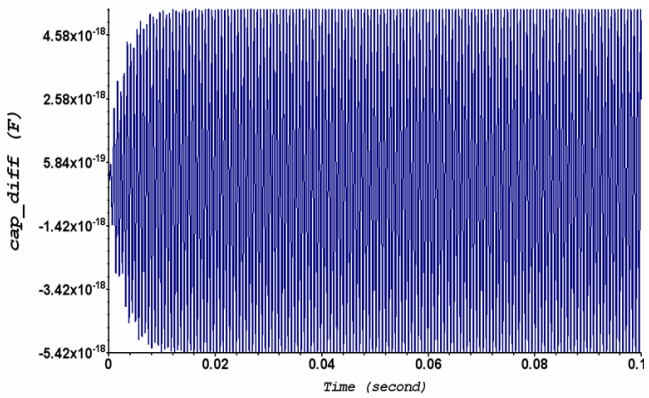

Fig. 13.SME Transient Results- Response of differential capacitance

VII. Conclusion

We successfully simulated 3-DoF Non-Resonant micromachined vibratory gyroscope using both FEA and System model extraction technique in TEM and SYNPLE Module of IntelliSuite. We found that by using SME technique we can quickly and easily optimize our device design through parametric analysis and using the high speed of the system level simulator SYNPLE. Thru this SME technique, device optimization took few hours as compare to FEA. We also found that this technique also gives comparative results as compare to FEA so we can rely on this technique for optimization of the device. For transient analysis, in SYNPLE we simulated our device for a total time of 0.1 second instead of 0.001 second for initial 6 cycles in FEA which were not sufficient to get full startup effect of the gyro. Time taken by FEA for this interval was around 45 hours whereas we got device transient responses using SME and SYNPLE in just two to three hours, almost 15 times faster than FEA. So this technique enables the users to optimize their device in much shorter time and they can quickly see that how their device will to react against certain parameters. Once device optimization gets complete in system level simulator then designer can carry out comprehensive FEA on the device to know its overall behavior.

Acknowledgment

This research was supported by Higher Education commission of Pakistan (HEC) funded by Indigenous 5000 fellowship program, IRSIP and NRPU. The authors thank Mathew Stevenson at Queens University, Kingston, ON, Canada and Mrs. Rubina Shaheen Sr. Scientist at ICCC Islamabad, for their excellent suggestions, help and guidelines during this course of studies.

References

[1] N. Yazdi, F. Ayazi, and K. Najafi. “Micromachined Inertial Sensors”. Proc. of IEEE, Vol. 86, No. 8, August 1998.

[2] W. Geiger, W.U. Butt, et al. “Decoupled Microgyros and the Design Principle DAVED” Sensors and Actuators A (Physical), Vol. A95, No.2-3, Jan. 2002, pp. 239-249.

[3] A. Shkel, R. T. Howe, & R. Horowitz, “Modeling and simulation of micromachined gyroscopes in the presence of imperfections,” Int. Conf. Modeling Simulation of Microsystems, Puerto Rico, 1999, pp. 605–608.

[4] Sung Kyu Ha, Hee Moon Jeong, Juno Kim “Robust of a Decoupled Vibratory Microgyroscope considering Over-Etching as a Fabrication tolerance factor” JSME International Journal Series A, Vol 42, No. 2, 2006, pp 273-281..

[5] A. Shkel, R. Horowitz, A. Seshia, S. Park and R.T. Howe. “Dynamics and Control of Micromachined Gyroscopes” American Control Conference, CA, 1999

[6] Said Emre Alper and Tayfun Akin “A Single-Crystal Silicon Symmetrical and Decoupled MEMS Gyroscope on an Insulating Substrate” Journal of Microelectromechanical Systems, VOL. 14, NO. 4, AUGUST 2005 pp 707-717

[7] V. Apostolyuk “Theory and Design of Micromechanical Vibratory Gyroscope” MEMS/NEMS Handbook, Springer, Vol. 1, 2006. pp 173-195.

[8] C. Acar ”Robust Micromachined Vibratory Gyroscopes” Ph.D. thesis, Dept. of MAE, University of California - Irvine 2004

[9] Instructional Manual, IntelliSuite MEMS System Simulation Tool “SYNPLE”, IntelliSense Corporation, February 2007.

[10] C. W. Dyck et al, “Parallel Plate Electrostatic Dual-Mass Oscillator” Proceeding of SPIE, SOE, CA, 1999.